Title
Multi-scale silica structures for improved HIV-1 Capsid (p24) antigen detection

Journal
Analyst, 141(13)

ISSN
0003-2654

Authors
Lin, Sophia
Hedde, Per Niklas
Venugopalan, Vasan
et al.

Publication Date
2016-06-20

DOI
10.1039/c6an00519e

Analyst

PAPER

View Article Online
View Journal | View Issue

Cite this: *Analyst*, 2016, **141**, 4181

Multi-scale silica structures for improved HIV-1 Capsid (p24) antigen detection

Sophia Lin,[a] Per Niklas Hedde,[b] Vasan Venugopalan,[a,b] Enrico Gratton[b] and Michelle Khine*[a,b]

Received 3rd March 2016,
Accepted 28th April 2016

DOI: 10.1039/c6an00519e

www.rsc.org/analyst

Silica (SiO_2) micro- and nanostructures fabricated with pre-stressed thermoplastic shrink wrap film have been shown to yield far-field fluorescence signal enhancements over their planar or wrinkled counterparts. The SiO_2 structures have previously been used for improved detection of fluorescently labelled proteins and DNA. In this work, we probe the mechanism responsible for the dramatic increases in fluorescence signal intensity. Optical characterization studies attribute the fluorescence signal enhancements to increased surface density and light scattering from the rough SiO_2 structures. Using this information, we come up with a theoretical approximation for the enhancement factor based off the scattering effects alone. We show that increased deposition thickness of SiO_2 yields improved fluorescence signal enhancements, with an optimal SiO_2 thin layer achieved at 20 nm. Finally, we show that the SiO_2 substrates serve as a suitable platform for disease diagnostics, and show improved limits of detection (LOD) for the human immunodeficiency virus type 1 (HIV-1) p24 antigen.

Introduction

Due to its high sensitivity and broad dynamic background, fluorescence is widely used as an optical readout method for different sensing applications, such as environmental monitoring,[1,2] live cell imaging,[3–5] and molecular diagnostics.[6,7] Efforts persist to increase the sensitivity of fluorescence-based methods, in particular for biological assays, as better detection sensitivity can lend itself to lower limits of detection. This has important implications for disease diagnostics, where improved limits of detection can result in earlier diagnosis, and therefore better prognosis. Work done to increase the sensitivity of fluorescence-based diagnostics include the use of nanomaterials such as quantum dots,[8,9] metallic nanostructures or nanoparticles,[10,11] and photonic crystals.[12,13] Drawbacks to these technologies include the need for expensive materials as well as complicated fabrication techniques. Furthermore, the resulting fluorescence enhancements derived from these technologies are often limited to near-field effects that require precise control at the nanometric scale.[14] These drawbacks limit the deployment of these technologies as inexpensive diagnostic tools.

Previously, we demonstrated the ability to create multi-scale SiO_2 micro- and nano-structures that yield robust, far-field fluorescence signal enhancements by leveraging the heat-induced retraction properties of low-cost commodity shrink wrap film.[15] Coating the pre-stressed polymer film with stiff materials results in the formation of multi-scale wrinkles when the film is shrunk by thermally heating it above its glass transition temperature.[16] By conjugating fluorescent biomolecules onto a SiO-coated film and shrinking, we achieved dramatic increases of the fluorescence intensity on our substrates. We observed up to 116-fold signal enhancements of fluorescently labelled streptavidin on the SiO_2 structures with improved signal-to-noise ratios over the glass control using a simple upright epifluorescence microscope. These values, along with the fluorescence signal increase (SI), a factor we defined to evaluate the effects of shrinkage on the substrate's fluorescence signal, significantly exceeded that expected from merely concentrating the molecules, which occurs when the substrate retracts biaxially.

We attributed the fluorescence signal enhancements to a combination of photophysical, optical, and concentration effects. This strategy was expanded upon by Sharma, *et al.*, who used the SiO_2 structures to enhance the fluorescence signal of hybridized DNA and to obtain lowered limits of detection for the model DNA hybridization assay.[17] Human immunodeficiency virus type 1 (HIV-1) is a lentivirus that causes the HIV infection. As of 2014, approximately 36.9 million people worldwide are living with HIV.[18] If left untreated, HIV eventually leads to acquired immunodeficiency syndrome (AIDS). Since 2000, 25.3 million people have died from AIDS-related illnesses.[18] HIV-1 diagnosis is essential for treating, monitoring,

[a]*Department of Chemical Engineering and Materials Science, University of California, Irvine, Irvine, CA 92697, USA. E-mail: mkhine@uci.edu*
[b]*Department of Biomedical Engineering, University of California, Irvine, Irvine, CA 92697, USA*

and preventing further transmission of the virus. The most common test for HIV-1 involves detection of HIV-1 antibodies using the conventional ELISA, and more recently, rapid diagnostic tests (RDTs). However antibodies for HIV-1 only are detectable in blood 3–4 weeks after infection, leaving a window of opportunity for HIV-1 transmission during acute infection when the amount of virus in the body is highest. The HIV-1 capsid antigen (p24) is present in the body quickly following HIV-1 infection, and presents itself as a suitable target for early HIV-1 detection.

Here, we report on follow-up studies done to further characterize the mechanism behind the fluorescence signal enhancements obtained on the SiO_2 structures. We study the size effects of the SiO_2 structures on the light scattering properties and resulting fluorescence signal enhancements. Furthermore, we demonstrate functionality of the SiO_2 structures for disease detection by using the SiO_2 structures as a platform to detect HIV-1 p24 antigen. The SiO_2 structures overcome the limitations described by previous methods such as geometric constraints and expensive fabrication techniques, and represent a robust and scalable platform for improved detection of target biomolecules with applications in disease diagnostics.

Materials and methods

Chemicals and reagents

Plain microscope glass slides with dimensions 25 × 75 × 1 mm, Nunc sealing tape, EZ-link NHS-LC-biotin, 1-ethyl-3-(3-dimethylaminopropyl)carbodiimide hydrochloride (EDC-HCl), *N*-hydroxysulfosuccinimide (Sulfo-NHS), and StartingBlock were purchased from ThermoFisher Scientific. (3-Animopropyl)trimethoxysilane (APTMS), poly(glutamic acid) (pGlu), and polyclonal rabbit anti-HIV-1 p24 antibody were purchased from Sigma-Aldrich. Monoclonal mouse anti-HIV-1 p24 antibody, HIV-1 p24 full length protein, and polyclonal goat anti-rabbit IgG H&L (Alexa Fluor 647) were purchased from Abcam. Tetramethylrhodamine isothiocyanate (TRITC)-conjugated streptavidin was purchased from Jackson ImmunoResearch, Inc. Pre-stressed polyolefin (PO) film (955-D) was obtained from Sealed Air Corporation.

Fabrication and fluorescent functionalization of the SiO_2 structures

The SiO_2 structures were fabricated as previously described.[15,17] Briefly, SiO_2 was sputtered onto clean pre-stressed polyolefin (PO) film using ion-beam deposition system (MODEL IBS/e, South Bay Technology, Inc.) for a select period of time. 1 min of sputter deposition time was measured to deposit a 1 nm thickness of material. The coated film was then heated for 3 min at T = 140 °C. Heating the coated film past its glass transition temperature causes the PO film to reflow and retract to ~5% of its original area. The stiff SiO_2 layer, which cannot shrink, instead buckles and folds, resulting in the formation of multi-scale SiO_2 structures. Functionalization of the SiO_2 structures with fluorescent molecules was done as previously described.[15] Prior to shrinkage of the SiO_2-coated PO film, the PO film was treated with 2% v/v APTMS in ethanol for 30 min. The surfaces were washed and cured overnight. 0.10 mg mL^{-1} of EZ Link LC-Biotin was reacted with the silane treated surface for 1 h, cleaned, and then incubated with 10 μg per mL streptavidin-TRITC. The bio-functionalized surfaces were then shrunk at 3 min at T = 140 °C. Functionalization of the PO film control without the SiO_2 structures followed the same procedure except the SiO_2 deposition step was omitted.

SEM characterization

Fabricated samples at different SiO_2 thicknesses were prepared for scanning electron microscopy (SEM) by first sputtering the substrates with 8.0 nm iridium (IBS/e, South Bay Technology). SEM images were then obtained using a 3 kV beam at 4 mm working distance (FEI Magellan 400 XHR Scanning Electron Microscope).

Reflectance measurements

UV-visible absorption spectra of the SiO_2 substrates were collected using a PerkinElmer Lambda 95 UV/Vis/NIR Spectrophotometer with the help of the Law group. For highly scattering surfaces, a 60 mm diameter integrating sphere was used. Clean PO films were sputtered with different thicknesses of SiO_2 (0, 5, 10, 20, 40 nm). The SiO_2-sputtered films were shrunk to create the multiscale SiO_2 structures. The reflectance spectra of the SiO_2 structures were collected from λ = 400–800 nm.

Pinhole scanning experiment

The pinhole scanning experiment of the bio-functionalized SiO_2 substrates was performed using laser confocal microscopy (Olympus FV1000) at the Laboratory for Fluorescence Dynamics (University of California, Irvine). The substrates were excited at λ = 559 nm and emission was collected at λ = 575–620 nm using a 20× objective (NA = 0.75). The emission of the fluorescently labelled substrates was collected as the pinhole was displaced in the x-plane in 100 μm steps. Confocal z-stacks (scan range 50 μm, 1 μm steps) of the fluorescently labelled substrates were also acquired using the same confocal setup. Fluorescence images with the pinhole open were taken using a 10× objective (NA = 0.40). Images were analyzed using ImageJ.

Widefield fluorescence imaging

Fluorescent images of the streptavidin-TRITC functionalized substrates were taken using a custom built upright fluorescence microscope (Olympus) using a 2× objective (NA = 0.055, Edmond Optics). Fluorescent images from the p24 immunoassay experiment was taken using an upright fluorescence microscope (Olympus) using a 5× objective (NA = 0.13, Olympus). Images were analyzed using ImageJ.

p24 immunoassay

The SiO_2-treated PO film and glass slide were immersed in 2% v/v APTMS for 30 min. The surfaces were rinsed, cured

overnight, and then incubated with pGlu (3 mg mL^{-1}) for 1 h at room temperature the next day. After washing with double deionized water (ddH_2O), the substrates were then incubated in EDC-HCl/Sulfo-NHS (75 mM/15 mM) solution for 1 h for protein crosslinking. 10 μg mL^{-1} of monoclonal mouse anti-HIV1 p24 antibody was conjugated onto the EDC-HCl/Sulfo-NHS activated surfaces by incubating the protein solution with the surfaces overnight at 4 °C. Surfaces were washed with 0.05% v/v PBST three times the next day to remove the excess antibodies and blocked with StartingBlock. Human HIV-1 p24 antigen was incubated with the surfaces overnight at 37 °C. Following capture of the target analyte, polyclonal rabbit anti-HIV1 p24 antibody was incubated with the surface for antigen–antibody recognition. Goat anti-rabbit IgG H&L (Alexa Fluor 647) was then incubated with the surfaces for final visualization of the p24 antigen. The primary and secondary antibody binding was carried out at 37 °C for 1 h. After the substrates were cleaned, the films were thermally shrunk at T = 140 °C.

Results

SiO_2 structure characterization

We fabricated SiO_2 substrates with different sized wrinkles and thicknesses by varying the SiO_2 deposition time. Sputter deposition times of 5, 10, 20, and 40 min were conducted resulting in pre-shrunk thin film thickness of 5, 10, 20, and 40 nm, respectively. Fig. 1 is a schematic illustrating the fabrication of the SiO_2 structures. SiO_2 is sputtered onto the surface of the PO film, creating a bilayer material.

Thermal heating of the SiO_2-coated PO film causes the pre-stressed polymer layer to retract and the stiff SiO_2 layer on the surface to buckle and fold, resulting in a hierarchical population of micro- to nano-scale SiO_2 structures. Fig. 2 are top down and cross-sectional SEM images of the resulting structures at different thicknesses of deposited SiO_2 following shrinkage of the coated PO film. Longer SiO_2 deposition times (therefore thicker thin films) result in larger feature wavelengths following film shrinkage, as predicted by the wrinkling equations. The thickness of the shrunk SiO_2 layer also increases, as verified with the laser scanning confocal microscope measurements, and the shrunk wrinkle heights are tabulated in Table 1.[19,20]

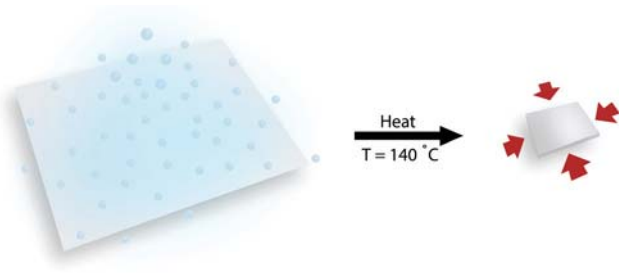

Fig. 1 Schematic illustrating the fabrication process of the SiO_2 structures. SiO_2 is sputtered onto the film surface, and shrunk thermally at T = 140 °C.

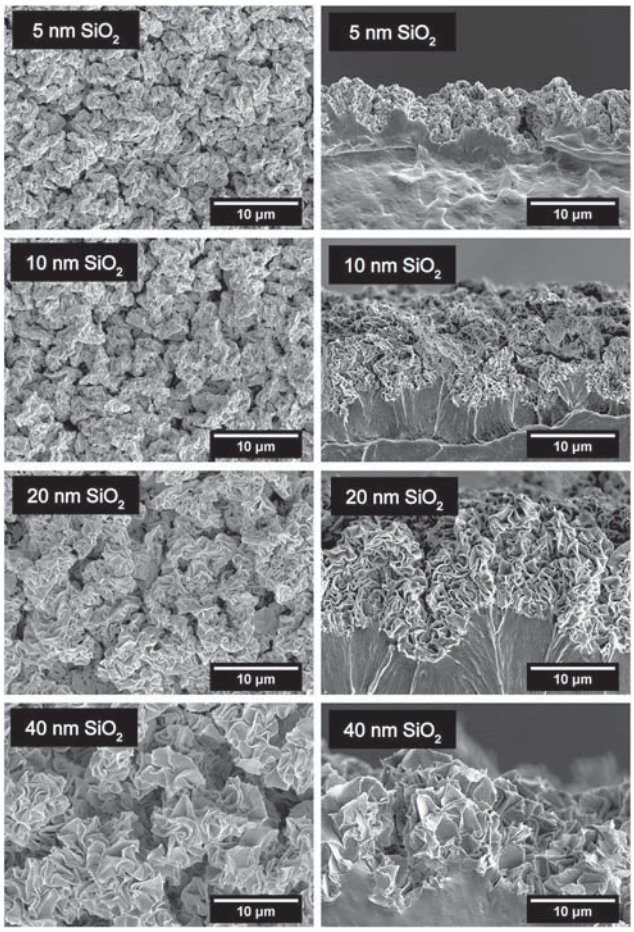

Fig. 2 SEM images of the SiO_2 structures formed from shrinking the SiO_2-coated (5, 10, 20, 40, nm) polymer film sputtered with different SiO_2 thicknesses (5, 10, 20, 40 nm) are shown, with the left hand column consisting of top down SEM images and the right hand column consisting of cross-sectional SEM images.

Table 1 Wrinkle thicknesses measured on the shrunk SiO_2-coated PO films

Deposited SiO_2 thickness (nm)	Shrunk wrinkle height (μm)
5	4.7 ± 0.2
10	6.4 ± 0.9
20	9.6 ± 1.3
40	10.6 ± 1.7

Integrating sphere measurements

We measured the reflectance and transmittance of the shrunk polymer substrates with different thicknesses of deposited SiO_2. The results are shown in Fig. 3. The graph reveals that the PO film is inherently reflective, which explains the increased fluorescence signal read on the flat, unshrunk

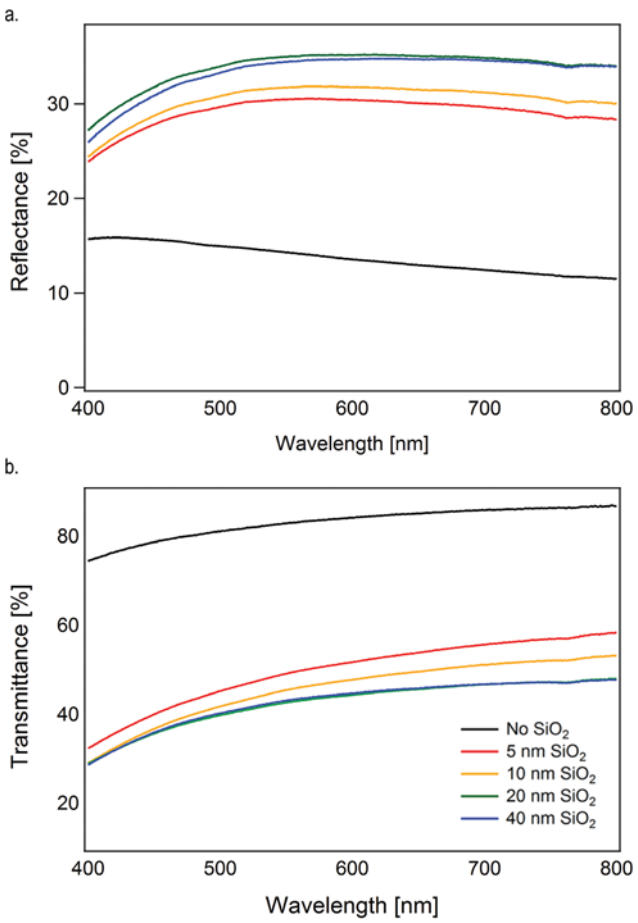

Fig. 3 Reflectance and transmittance spectra of the shrunk polymer substrates with different deposited thicknesses of SiO_2. The legend for both graphs are shown in the bottom right hand portion of the transmittance spectra.

fluorescently-conjugated PO film relative to the glass control. Furthermore, as the deposited thickness of SiO_2 increases from 5 nm to 40 nm, the shrunk substrate exhibits a higher percent reflectance (Fig. 3a). The increased reflectance upon the addition of the SiO_2 structures indicates that these multi-scale structures gives rise to additional light scattering resulting in reduced transmittance (Fig. 3b) and further increases in reflectance. Interestingly, the measured percent reflectance of the 20 nm and 40 nm deposited SiO_2 of transmittance and reflectance are similar, while incremental changes are observed from 0 nm to 20 nm deposited SiO_2 substrates.

Pinhole scanning experiment

We looked to confirm the reflective nature of the SiO_2 structures and therefore investigated the scattering properties of the SiO_2 surfaces through the scanning pinhole experiment. The scanning pinhole experiment capitalizes on the confocal microscope's ability to reject out-of-focus light. We prepared the substrates by first functionalizing the SiO_2-coated films with streptavidin-TRITC. We then thermally shrunk the surfaces to create fluorescently labelled SiO_2 structures. In this study, we repeatedly imaged the same region at different pinhole positions. By misaligning the detection pinhole, which exists to eliminate out-of-focus light, we expect to see significantly reduced fluorescence signal as the focal volume gets further away from the detector. The results from this experiment are plotted in Fig. 4, which is a graph of the normalized fluorescence intensity as a function of the pinhole misalignment. As expected, there is a drop in the collected emission as the detection pinhole becomes more misaligned for all substrates (0, 5, 10, 20, 40 nm SiO_2). More interestingly, Fig. 4 reveals that as we increase the SiO_2 thickness from 5 nm to 40 nm, a higher fluorescence emission is collected at each respective pinhole misalignment. The fluorescence decay due to pinhole misalignment slows down as the SiO_2 thickness increases until the SiO_2 thickness of 20 nm is reached. The collected fluorescence emission at 40 nm deposited SiO_2 follows a similar decay rate observed on the 20 nm substrates, suggesting a limit to the size or thickness effect on the emitted fluorescence intensity. Overall, more fluorescence emission on substrates with SiO_2 structures was collected through a misaligned detection pinhole. This suggests to us that the SiO_2 structures promote multiple scattering that serves to increase the axial extent of the fluorescence excitation and enhance both the availability of excitation light and backscattering of the fluorescence emission.

We then constructed *z*-stacks of the fluorescently labelled SiO_2 structures (20 nm SiO_2) and the shrunk PO film surface to further verify the scattering properties of the SiO_2 structures. Taking *z*-stacks served to eliminate fluorescence detection from outside the focal plane and quantify the fluorescence emission from individual *z*-slices. The results are shown in Fig. 5a, which is a graph of the fluorescence intensity of the functionalized surface as a function of distance throughout the substrate in the *z*-axis. Both fluorescently conjugated SiO_2 structures and shrunk PO film show similar trends throughout the sample and the integrated intensity reveal that

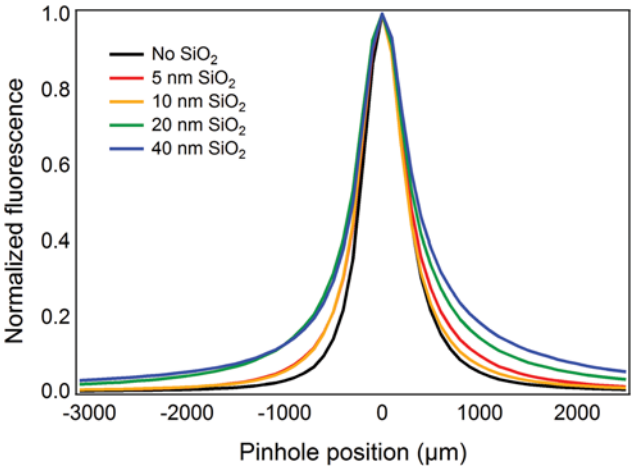

Fig. 4 Graphical illustration of the normalized fluorescence as a function of pinhole misalignment on substrates with different thicknesses of SiO_2.

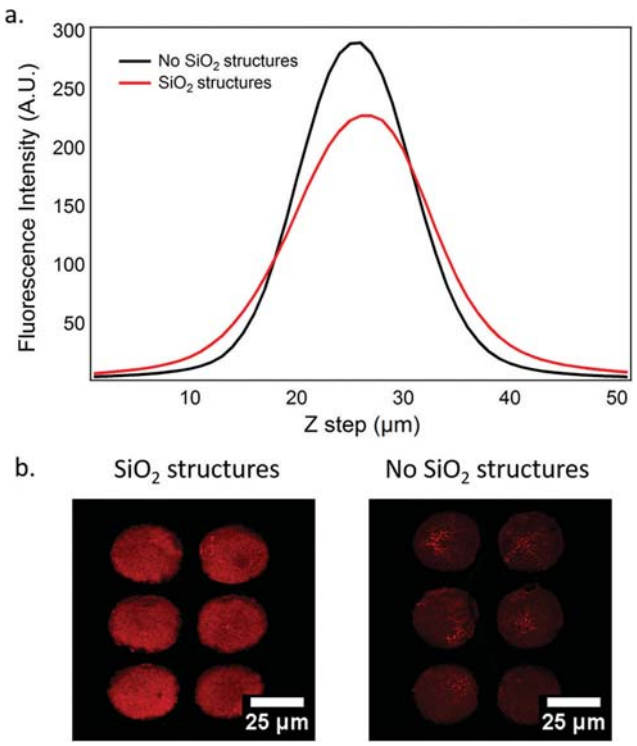

Fig. 5 Fluorescence imaging to characterize scattering effects of the SiO_2 structures. A confocal *z*-stack of fluorescently labelled substrates shows that the overall trend of fluorescence intensity across the *z*-axis is very similar between substrates with SiO_2 structures and without the SiO_2 structures (a). Integrated intensity across the substrate yields very similar total fluorescence intensity. Fluorescence images of the same substrate taken with an open confocal pinhole show that the substrates with SiO_2 structures have greater fluorescence intensity compared to the shrunk polymer film without SiO_2 structures (b).

the two substrates have very similar total intensity, where the integrated fluorescence intensity is about $(4 \pm 0.5) \times 10^3$ AU and $(4 \pm 0.2) \times 10^3$ AU on the SiO_2 structures and shrunk PO film, respectively. We opened the pinhole to collect all the emitted light, which includes back-scattered fluorescence emission emanating from outside the focal plane. The fluorescence images are shown in Fig. 5b, where the observed fluorescence on the SiO_2 structures (left) is greater than that on the shrunk PO film (right). The measured fluorescence intensity on the SiO_2 structures measures ~2.5-fold greater than that obtained on the shrunk PO film. This discrepancy between the detected fluorescence intensity from the integrated *z*-stacks and that measured from the wide-field image confirms that out-of-focus light contributes to the enhanced fluorescence signal.

Theoretical approximation

From the optical characterization studies, we concluded that the multi-scale SiO_2 structures represent a highly light scattering surface, with larger scattering effects as the deposited SiO_2 thickness is increased. We looked to estimate a theoretical scattering enhancement factor (SEF) based off of these effects. We attribute the enhancement to a combination of enhancements due to multiple scattering of the fluorescence excitation and both backscattering and detection of the fluorescence emission. This estimate is broken down in eqn (1):

$$\mathrm{SEF} = \left(\frac{\%R, n\mathrm{nm}_{\lambda,\mathrm{ex}}}{\%R, 0\mathrm{nm}_{\lambda,\mathrm{ex}}}\right) + \left(\frac{\%R, n\mathrm{nm}_{\lambda,\mathrm{em}}}{\%R, 0\mathrm{nm}_{\lambda,\mathrm{em}}}\right) \times \left(\frac{\text{collection solid angle}}{2\pi}\right) \quad (1)$$

where the $\%R,n\ \mathrm{nm}_{\lambda,\mathrm{ex}}$ is the percent reflectance of the substrate with *n* thickness of deposited SiO_2 at the dye's excitation wavelength, $\%R,0\ \mathrm{nm}_{\lambda,\mathrm{ex}}$ is the percent reflectance of the substrate with no SiO_2 structures at the dye's excitation wavelength, $\%R,n\ \mathrm{nm}_{\lambda,\mathrm{em}}$ is the percent reflectance of the substrate with *n* thickness of deposited SiO_2 at the dye's emission wavelength, $\%R,0\ \mathrm{nm}_{\lambda,\mathrm{em}}$ is the percent reflectance of the substrate with no SiO_2 structures at the dye's emission wavelength. The first term represents the enhancement due to the increased availability of excitation light due to the multiple scattering produced by the SiO_2 nanostructures. The second term represents the enhancement of fluorescence detection due to backscatter and collection by the microscope objective. The collection solid angle is a factor that accounts for the amount of fluorescence emission detectable by the microscope objective. The theoretical SEF for each substrate at different thicknesses of SiO_2 is calculated based off the reflectance data obtained from the integrating sphere measurements and tabulated in Table 2.

We verified the theoretical approximations for the SEF SiO_2-coated films (0, 5, 10, 20, 40 nm) were functionalized with STRITC using the previous described conditions and the experimental SEF for each substrate at each thickness of SiO_2 was calculated. The results are tabulated in Table 2. We observe increased fluorescence intensity on the shrunk surfaces with increased deposited SiO_2 as seen in Fig. 6. The SEF observed on the shrunk substrates with different SiO_2

Table 2 Increasing the thicknesses of deposited SiO_2 results in higher scattering enhancement factors (SEF)

Deposited SiO_2 Thickness (nm)	Theoretical SEF	Experimental SEF
0	—	—
5	2.1	1.0 ± 0.1
10	2.2	1.8 ± 0.2
20	2.4	2.3 ± 0.4
40	2.4	2.5 ± 0.5

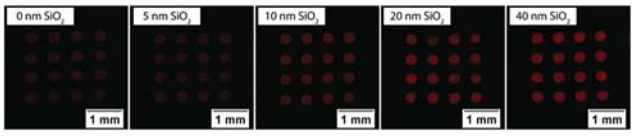

Fig. 6 Fluorescent intensity images of the shrunk fluorescently-conjugated polymer substrates at different deposited thickness of SiO_2.

structures are calculated from the fluorescence intensities and shown in Table 2. As we increase the deposited thin film thickness from 5 nm to 40 nm, the experimental SEF increased until it plateaus at 20 nm of deposited SiO_2. This trend follows that predicted by the theoretical SEF. The discrepancy at 5 nm of deposited SiO_2 can be attributed to discontinuities of the deposited thin film at that low of a thickness.

As we increase the deposited thin film thickness from 5 nm to 40 nm, the fluorescence intensity increases until it plateaus at 20 nm of SiO_2. This complements the results obtained in the pinhole scanning experiment, where increased SiO_2 thickness yielded higher scattering effects, with the maximal scattering achieved at 20 nm deposited SiO_2. The SEF on the deposited SiO_2 thickness can be explained through the wavelength equation, as shown in eqn (2), where λ is the resulting wrinkle wavelength, h is the thickness of the film skin layer, E_f and E_s are the elastic modulus of the film skin layer and substrate, respectively.[16,19]

$$\lambda \sim 2\pi h\left(\frac{E_f}{3E_s}\right)^{1/3} \quad (2)$$

Eqn (2) shows us that as the deposited SiO_2 film thickness increases from h = 5 to 40 nm, larger feature sizes are obtained on the shrunk polymer substrates. This is confirmed through the SEM images in Fig. 2 and the height measurements of the shrunk SiO_2 layer in Table 1. Larger wrinkles have more surface area available to scatter light, and the multiple scattering effects that occur produce diffuse light that increases the light available for fluorescence excitation and subsequently emission rate of attached fluorophores. A limit to the SEF appears to be reached at 20 nm of deposited SiO_2, and this may be due to increased density of SiO_2 structures affecting the fluorescence scattering efficiency. Further studies need to be done to characterize this limit.

Improved detection of the p24 antigen

Previously, we showed the SiO_2 structures were a suitable platform for improved limits of detection of fluorescently labelled protein.[15] Sharma *et al.* also used the SiO_2 structures for DNA hybridization assays with increased detection sensitivity.[17] Here, we demonstrate that the SiO_2 structures are amenable to disease diagnostic applications through detection of the HIV-1 p24 antigen. We constructed a sandwich immunoassay with a fluorescence-based readout method for the HIV-1 p24 antigen onto the SiO_2 structures by first incubating the surfaces (here, the preshrunk SiO_2-coated film and a planar glass surface) with monoclonal mouse anti-HIV1 p24 antibody. HIV-1 p24 antigen with concentrations ranging from 1 pg mL^{-1} to 200 pg mL^{-1} were applied to the surfaces. The target analyte was detected using polyclonal rabbit anti-HIV1 p24 antibody, and visualized using secondary antibody polyclonal goat anti-rabbit IgG H&L (Alexa Fluor 647). The immunoassay scheme is shown in Fig. 7. After the secondary antibody is applied, the substrates were thermally shrunk and wide-field fluorescence intensity images were taken.

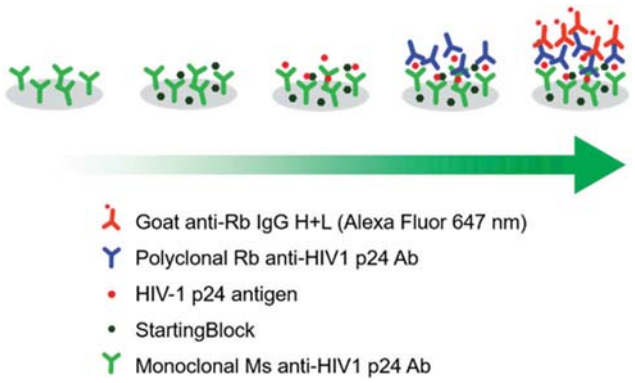

Fig. 7 Schematic illustrating the p24 sandwich immunoassay performed on the SiO_2-coated film prior to shrinkage. After incubation with the secondary antibody, the entire substrate is shrunk.

The results are shown in Fig. 8, which is a concentration curve of the fluorescence intensity as a function of HIV-1 p24 antigen concentration. The values are averaged across independent experiments (n = 3), and the errors are calculated to be the standard error. We note that amplification upon substrate shrinkage not only results in increased signal, but also an increase in the error. The limit of detection (LOD) is determined at 3 standard deviations above the background, and we observe improved LOD on the SiO_2 structures (30 pg mL^{-1}) over the planar glass substrate (253 pg mL^{-1}). 10 pg mL^{-1} of p24 was reported to be detectable through ELISA.[21]

We observe improved LOD on the SiO_2 structures over the planar glass control. We anticipate with surface chemistry optimization and/or improvement of the reflective nature of our SiO_2 structures, our p24 assay platform will surpass limits obtained using the standard ELISA. Furthermore, the SiO_2 sensing platform offers the potential for multiplexing as we have demonstrated improved DNA hybridization assay

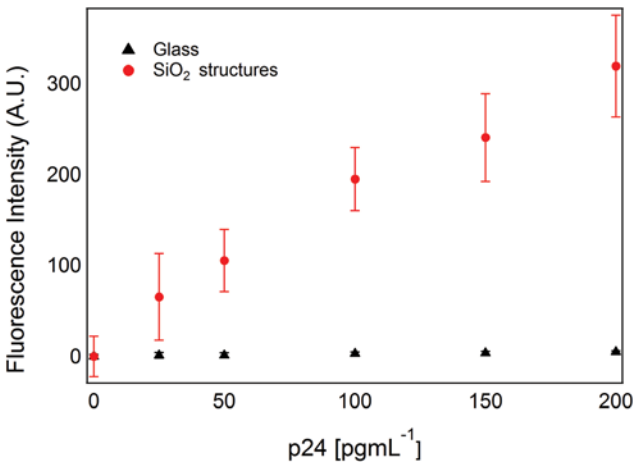

Fig. 8 Graphical illustration of p24 concentration curve, where the fluorescence intensity on the glass substrate is represented by the black triangles, and the fluorescence intensity on the SiO_2 structures is represented by the red circles.

performance on the SiO_2 structures.[17] Other biomarkers such as HIV RNA and the antibodies specific to HIV arise in the body as the disease progresses. Therefore, the SiO_2 structures can be used to not only diagnose HIV during the acute infection stage, but it also be used as a versatile platform for both RNA and HIV antibody sensing following the acute infection stage. This is advantageous since traditional ELISA assays are limited to protein detection.

Conclusions

We previously showed that shrinking fluorescently labelled SiO_2-coated shrink wrap film yielded significantly higher fluorescence signals compared to that observed from shrinking a fluorescently labelled polymer film.[15] Here, we report on the mechanism behind the dramatic fluorescence signal enhancements achieved on the SiO_2 substrates. From the optical characterization studies, we ascribed the enhanced fluorescence signals to the scattering nature of the rough SiO_2 structures, and we came up with a theoretical approximation for the fluorescence enhancement based off these scattering effects (SEF). We verified the approximation with experimental results to show that the deposited SiO_2 thickness dictates the fluorescence signal intensities achievable on the structures. The porous SiO_2 structure geometry that arises following polymer film shrinkage causes diffuse scattering, with thicker SiO_2 thin films (therefore larger fabricated features) scattering more light. The increased local light field results in higher rates of both absorption and fluorescence emission.

The enhanced fluorescence signals obtained are robust and far-field, and we showed that the SiO_2 substrates are amenable to disease diagnostic applications with lowered LOD achieved on the SiO_2 structures (30 pg mL^{-1}) over planar controls (253 pg mL^{-1}) for the p24 antigen. Many studies demonstrating improved LOD for the HIV1 p24 antigen over the traditional ELISA have been reported, yet drawbacks to these methods persist and hamper translation of these methods towards clinical use.[22–24] A nanoparticle-based bio-barcode amplification assay is able to detect HIV1 p24 antigen concentrations down to 0.1 pg mL^{-1}. This method, which couples an immunoassay with PCR amplification, requires subsequent PCR amplification steps in order to achieve such low sensitivity.[25] Another study used inductively coupled plasma mass spectrometry to quantify p24 antigen detection (LOD = 1.49 pg mL^{-1}).[26] Improved detection sensitivity typically correlates with increased assay complexity.

Traditional ELISAs, which are considered the gold standard, have a relatively high LOD at 10 pg mL^{-1}. Though our reported LOD falls within the same order of magnitude, we anticipate surface chemistry optimization and improvement of the reflective nature of our SiO_2 structures will allow our p24 assay platform to surpass limits obtained using the standard ELISA. Further work is required for optimization of the SiO_2-based sensors. Our method requires high temperatures in order to achieve shrinkage, limiting it to an endpoint assay. A potential strategy to overcome this involves using a low-temperature polymer shrink film. Additionally, a limit in the fluorescence enhancements is observed here at 20 nm of SiO_2. Further studies are required to characterize the surface area available for multiple light scattering events and to optimize the substrates for greater fluorescence enhancements. Despite these limitations, the SiO_2-based platform offers many advantages. The SiO_2 structures are simple to fabricate and eliminate many processing steps associated with traditional nanostructure fabrication methods. We can pattern at the large scale and then shrink to create the SiO_2 structures that yield robust, far-field fluorescence signal enhancements that are not limited to the near-field and are wavelength independent. We have demonstrated the SiO_2 structures are able to enhance the detection sensitivity of both DNA and protein assays, suggesting the possibility of multiplexing. Additionally, the platform is scalable: we have shown the ability to deposit similar thin films through roll-to-roll manufacturing for fabrication of micro- and nanostructures.[27] Therefore, these SiO_2 substrates represent a potentially new and scalable tool for surface sensing applications.

Acknowledgements

This work was supported by the National Institute of Health (NIH) DP2 NIH Director's New Innovator Award (1 DP2 OD007283-01) and the National Science Foundation Biophotonics across Energy, Space, and Time (BEST) IGERT Program (NSF-DGE-1144901). EG and PNH acknowledge support from NIH grants NIH P41-GM103540 and NIH P50-GM076516. VV acknowledges support from the Laser Microbeam and Medical Program, NIH grant P41-EB015890. SEM work was performed at the UC Irvine Materials Research Institute (IMRI). Special thanks to Sun-Jun Park for his help in sample preparation for cross-sectional SEM imaging.

References

1 Y. Jeong and J. Yoon, *Inorg. Chim. Acta*, 2012, **381**, 2–14.
2 H. N. Kim, W. X. Ren, J. S. Kim and J. Yoon, *Chem. Soc. Rev.*, 2012, **41**(8), 3210.
3 M. J. Ruedas-Rama, J. D. Walters, A. Orte and E. A. H. Hall, *Anal. Chim. Acta*, 2012, **751**, 1–23.
4 K. P. Carter, A. M. Young and A. E. Palmer, *Chem. Rev.*, 2014, **114**, 4564–4601.
5 X. Michalet, F. F. Pinaud, L. A. Bentolila, J. M. Tsay, S. Doose, J. J. Li, G. Sundaresan, A. M. Wu, S. S. Gambhir and S. Weiss, *Science*, 2005, **307**(5709), 538–544.
6 W. RussAlgar, M. Massey and U. J. Krull, *TrAC, Trends Anal. Chem.*, 2009, **28**(3), 292–306.
7 K. K. Jain, *Clin. Chim. Acta*, 2005, **358**(1–2), 37–54.
8 Y. Xing and J. Rao, *Cancer Biomarkers*, 2008, **4**(6), 307–319.
9 Y. Zhang and T. H. Wang, *Theranostics*, 2012, **2**(7), 631–654.
10 D. Liu, Z. Wang and X. Jiang, *Nanoscale*, 2011, **3**(4), 1421–1433.

11 Y. Zhang, W. Chu, A. Foroushani, H. Wang, D. Li, J. Liu, C. Barrow, X. Wang and W. Yang, *Materials*, 2014, **7**(7), 5169–5201.
12 A. Pokhriyal, M. Lu, V. Chaudhery, C.-S. Huang, S. Schulz and B. T. Cunningham, *Opt. Express*, 2010, **18**(24), 24793–24808.
13 N. Ganesh, W. Zhang, P. C. Mathias, E. Chow, J. a. N. T. Soares, V. Malyarchuk, A. D. Smith and B. T. Cunningham, *Nat. Nanotechnol.*, 2007, **2**(8), 515–520.
14 A. Kinkhabwala, Z. Yu, S. Fan, Y. Avlasevich, K. Müllen and W. E. Moerner, *Nat. Photonics*, 2009, **3**(11), 654–657.
15 S. Lin, H. Sharma and M. Khine, *Adv. Opt. Mater.*, 2013, **1**(8), 568–572.
16 C. C. Fu, A. Grimes, M. Long, C. G. L. Ferri, B. D. Rich, S. Ghosh, S. Ghosh, L. P. Lee, A. Gopinathan and M. Khine, *Adv. Mater.*, 2009, **21**, 4472–4476.
17 H. Sharma, J. B. Wood, S. Lin, R. M. Corn and M. Khine, *Langmuir*, 2014, **30**(37), 10979–10983.
18 UNAID Fact Sheet 2015, 2015.
19 K. Efimenko, M. Rackaitis, E. Manias, A. Vaziri, L. Mahadevan and J. Genzer, *Nat. Mater.*, 2005, **4**(April), 293–297.
20 J. Yin and C. Lu, *Soft Matter*, 2012, **8**(24), 6528.
21 P. Fan, X. Li, W. Su, W. Kong, X. Kong, Z. Wang, Y. Wang, C. Jiang and F. Gao, *PLoS One*, 2015, **10**(4), e0125701.
22 K. Teeparuksapun, M. Hedström, E. Y. Wong, S. Tang, I. K. Hewlett and B. Mattiasson, *Anal. Chem.*, 2010, **82**, 8406–8411.
23 R. de la Rica and M. M. Stevens, *Nat. Nanotechnol.*, 2012, **8**(9), 1759–1764.
24 Y.-S. Fang, X.-J. Huang, L.-S. Wang and J.-F. Wang, *Biosens. Bioelectron.*, 2015, **64**, 324–332.
25 H. Dong, J. Liu, H. Zhu, C.-Y. Ou, W. Xing, M. Qiu, G. Zhang, Y. Xiao, J. Yao, P. Pan and Y. Jiang, *Virol. J.*, 2012, **9**(1), 180.
26 Q. He, Z. Zhu, L. Jin, L. Peng and S. Hu, *J. Anal. At. Spectrom.*, 2014, **29**, 1477–1482.
27 J. M. Nokes, R. Liedert, M. Kim, A. Siddiqui, M. Chu, E. Lee and M. Khine, *Materials*, 2015, **9**(3), 1–25.